Bifurcation, Bursting and Spike Frequency Adaptation

JOHN GUCKENHEIMER *

gucken@cam.cornell.edu

Mathematics Department and Center for Applied Mathematics, Cornell University, Ithaca, NY 14853

RONALD HARRIS-WARRICK *

rmh4@cornell.edu

Section of Neurobiology and Behavior, Cornell University

JACK PECK *

jhp6@cornell.edu

Department of Psychology, Ithaca College, Ithaca, NY 14850

ALLAN WILLMS *

arwillms@cam.cornell.edu

Center for Applied Mathematics, Cornell University

Abstract. Many neural systems display adaptive properties that occur on time scales that are slower than the time scales associated with repetitive firing of action potentials or bursting oscillations. *Spike frequency adaptation* is the name given to processes that reduce the frequency of rhythmic tonic firing of action potentials, sometimes leading to the termination of spiking and the cell becoming quiescent. This paper examines this processes mathematically, within the context of *singularly perturbed dynamical systems*. We place emphasis upon the lengths of successive interspike intervals during adaptation. Two different bifurcation mechanisms in singularly perturbed systems that correspond to the termination of firing are distinguished by the rate at which interspike intervals slow near the termination of firing. We compare theoretical predictions to measurement of spike frequency adaptation in a model of the LP cell of the lobster stomatogastric ganglion.

1. Introduction

Spike frequency adaptation is the gradual slowing of the rate of firing in a neuron (Hille 1992). This definition of spike frequency adaptation allows multiple physiological bases. When spike frequency adaptation leads to the termination of spiking or to bursting oscillations, there are also multiple dynamical mechanisms that may be associated with this termination. There has been substantial interest in the qualitative classification of bursting oscillations of electrophysiological systems (Rinzel 1987, Bertram et al. 1995, Wang and

Rinzel 1995) based upon the theory of singularly perturbed systems of differential equations and bifurcation theory of dynamical systems. These descriptions have been formulated from the viewpoint of singularly perturbed systems as "slowly varying" dynamical systems. In this approach, two time scales are identified in the models. The faster time scale captures the dynamics associated with periodic firing while the adaptive properties are described by modulation of the firing that occurs on the slower time scale. The slowly varying point of view fixes the unit time scale as a fast time and regards adaptation as the movement of parameters for the fast subsystem through its parameter space. When the separation between these time scales is infinite, the "frozen" system

is a family of vector fields in which the slowly varying variables become parameters for the fast subsystems that no longer evolve. To interpret time series recordings that display spike frequency adaptation in terms of the frozen system, the series can be divided into temporal epochs in which the dynamics are governed by a particular attractor of the fast dynamical system. The transitions between these attractors are bifurcations of the frozen system. The same analysis applies to both the termination of spiking through spike frequency adaptation and to the repetitive terminations of spiking that occur in bursting oscillations. In both cases, the classification of bifurcations that terminate a family of limit cycles can be used to elucidate the dynamical mechanisms underlying spike termination.

Application of bifurcation theory to the analysis of transitions between spiking and quiescent behavior of a neural system is a pattern recognition problem. Bifurcations are associated with characteristic features of time series from voltage traces. Qualitative features of the traces such as decaying or growing oscillations, action potentials that overshoot or undershoot, etc. can be used to establish which types of bifurcation are consistent with the observations (Bertram et al. 1995). Thus the classification of bursting oscillations proceeds in two stages: identification of significant qualitative features in time series and association of bifurcations with the identified complex of features. This process is imperfect for a variety of reasons, including ambiguous data and the possibility that the identified features do not uniquely determine a single underlying dynamical mechanism. Our thesis in this paper is that quantitative analysis of sequences of interspike intervals provides additional information that can be used to constrain the mechanisms underlying the termination of spiking. The methods are most useful in situations where the active phase of an oscillation has a large number of action potentials. This assumption is satisfied by generic systems in the singular limit of widely separated time scales that is used in the formulation of the qualitative theory. The mathematical theory of singularly perturbed systems is currently inadequate to provide rigorous foundations for our quantitative analysis. There is a lack of theory describing the transitions

that occur in systems that have periodic attractors in their fast subsystems; existing literature deals primarily with transitions from stable equilibria of the fast subsystems (Mishchenko and Rozov 1980, Nejshtadt 1985). This paper outlines initial steps toward such a quantitative theory, though we give no pretense of mathematical rigor and minimize the technicality of our mathematical descriptions.

Our ultimate goal is a reliable set of methods that enable one to associate dynamical mechanisms between periodic spiking and quiescent behavior in data from neural systems. Accomplishing this goal requires an assessment of the robustness of our data analysis methods when applied to experimental data that is noisy. To examine these questions, we study data from an isolated LP neuron of the stomatogastric ganglion and a moderately realistic conductance based model for this neuron. There are some surprises that occur in the analysis of the model neuron. We identify transition behavior in the model neuron distinctly different from that previously described. The transition is associated with subcritical Hopf bifurcation, but it differs from the "Type III" bursting behavior described by Rinzel (1987) and Bertram et al. (1995). It also differs from the bursting oscillations with subcritical Hopf bifurcations studied by Rinzel and Troy (1982) and Ermentrout and Kopell (1986). Aspects of the experimental data that we analyze show features reminiscent of this new Hopf bifurcation scenario. We give a brief description of this new type of transition and extend our quantitative analysis to include this case.

Section 2 of this paper is a mathematical discussion of mechanisms by which periodic spiking ceases in systems with two widely separated time scales. We focus attention on cases in which the interspike intervals increase without bound as they approach the termination of spiking and the separation between time scales becomes larger. Extending the observations of Rinzel and Ermentrout (1989), we study the rate at which the interspike intervals grow in terms of the ratio between the time scales. Our analysis is applied to numerical data from the model discussed in Rinzel and Ermentrout (1989). In Section 3, we investigate a larger conductance based model based upon voltage clamp data from the LP neuron of the stomatogastric ganglion (Harris-Warrick et al.

1995, Buchholtz et al. 1992). In some parameter ranges, we find that the dynamical mechanisms for spike frequency termination discussed in Section 2 fit the numerical data well, but there are other regions in which we find additional mechanisms for spike frequency termination. These new mechanisms entail subthreshold oscillations whose growth rate increases from cycle to cycle in the slowly varying system. Section 4 compares the results of our numerical investigations with measurements of interspike intervals from the LP neuron of *Panulirus interruptus* in which spike frequency adaptation leads to the termination of firing. In this section and the discussion in Section 5, we compare the experimental data with the different dynamical mechanisms for spike frequency adaptation discussed in the paper and argue that the subcritical Hopf mechanism introduced in this paper fits some of the experimental data better than the other scenarios we describe. Our conclusions are tentative, but we demonstrate the ability of our analysis to make distinctions among dynamical mechanisms for termination of spiking in neuronal data.

2. Dynamical Systems with Multiple Time Scales

Rinzel (1987) has emphasized the use of dynamical systems with two time scales to model bursting phenomena in electrically active cells. His analysis and its subsequent extensions (e.g. Bertram et al. 1995, Wang and Rinzel 1995) have not placed much emphasis upon the rigorous or quantitative analysis of systems with multiple time scales. The theory that underlies such analysis is only partially developed, and we develop it further to describe quantitative properties of transitions in multiple time scale systems that are subsequently used to relate experimental data to bifurcation mechanisms in models. Our focus is on scaling properties of interspike intervals at transitions associated with homoclinic, saddle-node and Hopf bifurcations. This section describes these mathematics.

We study systems of differential equations in R^{m+n} of the form

$$\begin{aligned} \dot{x} &= \epsilon f(x, y) \\ \dot{y} &= g(x, y) \end{aligned}$$

A system of differential equations written in this form is called a *singularly perturbed* vector field. Here $\epsilon \geq 0$ is a small parameter that explicitly separates the time scales of two sets of variables, the *slow* x variables, and the *fast* y variables. We call the system with $\epsilon = 0$ the *frozen* field. In the frozen field, the slow x variables do not evolve at all, but remain constant since $\dot{x} = 0$. The dependence of the system on ϵ makes it possible to study the behavior of the system for small ϵ in terms of the frozen field. The system $\dot{y} = g(x, y)$ is called the fast subsystem. In the frozen system, x acts as a set of parameters for the fast phase variables y while in the "thawed" system, the x variables evolve on a slower time scale than the fast variables. Thus we imagine that the fast variables approach an attracting state, but that this attracting state changes slowly in time. If the attracting state undergoes a bifurcation, then the system has a *transition* from one type of attracting state to another; in the examples we analyze here, the process of adaptation leads to a transition between tonic spiking and quiescence.

In our application to neural systems, there are several distinct time scales: the millisecond time scale associated with action potentials, the 10-500 millisecond time scale associated with the period of tonic firing, the 1 second time scale of bursting oscillations, and a 10-100 second time scale associated with adaptive properties of the cell that leads to termination of tonic spiking. Our slow time scale will be the slow time scale of this adaptation, and the frozen systems are capable of bursting, spiking or quiescent behavior depending upon the values of system parameters and slow variables. As has become customary in studies of Hodgkin-Huxley like models of neurons, we regard the fastest time scale (activation of the spike generating sodium channel) as instantaneous. The slow variables are regarded as moving the fast subsystem in an extended parameter space that includes the slow variables, modulating the behavior of the system in a state dependent fashion. Abrupt transitions between spiking and quiescent behavior occur close to bifurcations of the frozen system. Our goals are to classify "generic" cases of this transition and to determine asymptotic properties of the lengths of interspike intervals as the system undergoes the transition from tonic spik-
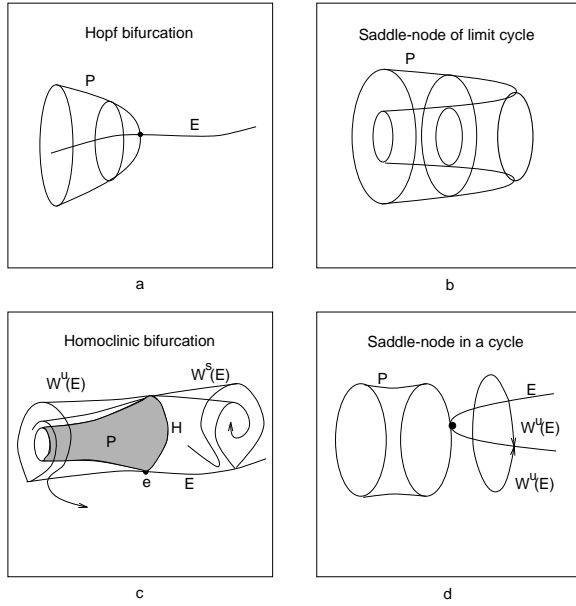
Fig. 1. Diagrams of generic codimension one bifurcations that lead to the birth or death of stable periodic orbits. In each case, the parameter varies along a horizontal axis and elements of phase portraits are drawn in vertical planes. The equilibrium curves are labeled E and the families of periodic orbits are labeled P. a) Hopf bifurcation, with a family of periodic orbits emerging from a curve of equilibrium points. b) branches of stable and unstable periodic orbits collide in a saddle node of limit cycles. c) a homoclinic bifurcation of a curve of saddle points. The stable and unstable manifolds of the equilibria, $W^s(E)$ and $W^u(E)$, pass through each other in the homoclinic orbit H. Trajectories in $W^u(E)$ have arrows. The front of the surface P of periodic orbits is shaded. d) a saddle-node in a cycle bifurcation. A curve of equilibria is born inside a cylinder formed from attracting invariant curves of the flow. These equilibria destroy the periodic orbits, the invariant curves then being formed from the unstable manifolds $W^u(E)$ of the unstable equilibria. The insets give an alternate depiction of the systems. Equilibrium points (stable - heavy line, unstable - dotted line) and extreme values of periodic orbits (stable - continuous line, unstable - dashed line) are projected into a plane in which the horizontal coordinate is the parameter and the vertical coordinate is one of the phase space variables.

ing to quiescence. Similar transitions mark the end of the active phase of bursting oscillations, but on somewhat faster time scales than those associated with the spike frequency adaptation studied in this paper.

The model analog of spiking behavior of a neuron is a stable periodic orbit of a dynamical system. We are interested in the ways in which a family of stable periodic orbits can terminate with a varying parameter or the variation of the slow variable(s) in a singularly perturbed system. Bifurcation theory (Guckenheimer and Holmes, 1983) classifies four general mechanisms for such transitions in generic families of vector fields, illustrated in Figure 1:

1. Hopf bifurcations
2. Saddle-nodes of limit cycles
3. Homoclinic bifurcations
4. Saddle-nodes of equilibria interrupting limit cycles

At Hopf bifurcations, a family of periodic orbits meets a family of equilibrium points. The amplitude of the oscillations of the periodic orbits decrease as the bifurcation point is approached as shown in Figure 1a. At saddle-nodes of limit cycles, a pair of periodic orbits of finite amplitude and period, but differing stability properties approach each other and annihilate each other as shown in Figure 1b. Families of periodic orbits can also terminate by the period of the periodic orbits growing without bound. This happens both in homoclinic bifurcations and at some saddle-node bifurcations of equilibria. Homoclinic orbits are defined to be trajectories that approach the same equilibrium point in both forwards and backwards time; i.e., they lie in both the stable and unstable manifolds of the saddle. At homoclinic bifurcations, the periods of a family of periodic orbits becomes unbounded as the periodic orbits tend to a homoclinic orbit as shown in Figure 1c. When a stable periodic orbit approaches a saddle-node of an equilibrium, the equilibrium point at the bifurcation has an open region of trajectories that converge to it. This region of trajectories contains the limit of the periodic orbit. Following the bifurcation, there are two equilibria, a sink and a saddle as shown in Figure 1d. The result is an excitable system in which perturbations that move an initial point from the sink to the opposite side of the saddle result in a trajectory that approximates the vanished periodic orbit.

What are the distinguishing characteristics of each of these types of transition in voltage recordings from neurons undergoing adaptation from a tonic to a quiescent state? We assume that observed spiking corresponds to following a continuous family of stable periodic orbits in a model system. Based on this assumption, Hopf bifurcations could be identified by the amplitude of the

oscillations decaying to zero. However, the multiple time scales in our "fast" subsystems can yield a very steep decline in amplitude of the oscillations (the *canard* phenomenon, Arnold et al 1994), and the continuous reduction in amplitude may not be readily discernible. Saddle-node bifurcations of limit cycles are characterized by the fact that the period of the oscillations remains bounded and the amplitude of the oscillations does not decay to zero. Separating the homoclinic and saddle-node bifurcations of equilibria using experimental data is more difficult. As observed by Rinzel and Ermentrout (1989), the asymptotic properties of the period of the oscillatory phase just prior to quiescence differ in these two cases. One of our objectives in this paper is to explore this observation more deeply and use it as the basis for distinguishing homoclinic bifurcations from saddle-node bifurcations that interrupt limit cycles. The remainder of this section outlines the mathematical analysis associated with the termination of firing behavior at homoclinic and saddle-node transitions in singularly perturbed systems.

Homoclinic orbits of a frozen system: The starting point for a systematic asymptotic analysis of homoclinic bifurcations in singularly perturbed systems is the geometric singular perturbation theory of Fenichel (1971). A homoclinic orbit approaches an equilibrium point e along its stable manifold as $t \to \infty$ and along its unstable manifold as $t \to -\infty$. In a generic frozen system with a homoclinic orbit, the equilibrium point e lies in a manifold E of equilibria for the fast system that are hyperbolic saddles. (See Figure 1c.) The stable manifolds of the equilibria in E fit together to form the stable manifold $W^s(E)$ of E. Similarly, the unstable manifolds of the equilibria form the unstable manifold $W^u(E)$ of E. Now $W^s(E)$ and $W^s(E)$ intersect transversally at the homoclinic orbits of equilibria in E. Furthermore, there is a family of periodic orbits P that lie to one side of H. The front of the surface P is shaded in Figure 1c. The periods of the orbits in P become unbounded as they approach H. Fenichel proves that much of this structure persists in the unfrozen system for $\epsilon > 0$. The manifold E is the limit of a family of normally hyperbolic manifolds E_ϵ as $\epsilon \to 0$. There are stable and unstable manifolds

for E_ϵ that continue to intersect transversally. In a neighborhood of E, Fenichel defines coordinates for which the families of (local) strong stable and unstable manifolds lie in coordinate planes.

We want to estimate the periods of periodic orbits of vector fields that pass close to a saddle point. In the vicinity of the saddle, the speed of the vector field is slow. If the periodic orbit comes close enough to the saddle, then the passage time past the saddle occupies most of the period. The relationship between the time required to pass by the saddle and the distance to the saddle is readily quantified in the case that the vector field is linear near the saddle. The theory established by Ilyashenko and Yakovenko (1991) allows us to introduce such coordinates for generic systems. More concretely, there are coordinates so that the saddle point for the fast subsystem is the origin and that the fast equations are defined by $\dot{y}_i = \lambda_i(x)y_i$ near the origin where the $\lambda_i(x)$ are smooth functions of the slow variable defining the eigenvalues of the saddle. Assume that $\lambda_i(x) > 0$ for $i = 1, \ldots, u$ and that $\lambda_i(x) < 0$ for $i = u + 1, \ldots, n$. The stable manifold of the origin is the coordinate subspace associated with indices $i = u + 1, \ldots, n$. The unstable manifold is the subspace associated with indices $i = 1, \ldots, u$. In each unstable direction, $y_i(t)$ is given by $y_i(0)\exp(t\lambda_i)$, implying that the time a trajectory spends near the origin is comparable to $\min(-\ln(y_i)/\lambda_i)$, $i = 1, \ldots, u$. From this estimate, we conclude that the period of a periodic orbit passing close enough to a saddle is proportional to the logarithm of the distance of its closest approach to the stable manifold. For a tonically firing neuron, the next paragraph demonstrates how this analysis leads to circumstances in which the period of firing is proportional to the logarithm of the time to termination.

Homoclinic transitions in a singularly perturbed system: A full asymptotic analysis of what happens to homoclinic orbits and nearby trajectories in singularly perturbed systems has not been performed, and we do not give a complete analysis here. Instead, we assume that there is a single slow variable x, and that we analyze trajectories of the singularly perturbed system that track a one parameter family of stable periodic or-

bits of the frozen system until it reaches the vicinity of a homoclinic orbit. This only makes sense for positive values of ϵ since trajectories of the frozen system do not pass through the homoclinic transition. Time is measured in "fast" time and we assume that x evolves at unit rate in slow time, i.e, $\dot{x} = \epsilon$ is constant and $f(x, y) \equiv 1$. To measure the period of the cycles n a trajectory of the singularly perturbed system, choose a cross section to the family of periodic orbits of the frozen system and measure the return time from one intersection with the cross section to the next. Each cycle of the oscillation of the singularly perturbed trajectory will carry it closer to the stable manifold of the invariant manifold corresponding to the frozen saddle points. Thus successive cycles of the oscillation grow longer. Since $\dot{x} = \epsilon$ is constant, the change in the slow variable x increases from one cycle to the next. Consequently, the successive periods of the oscillations grow a bit faster than logarithmically as would be expected if the distance to the homoclinic bifurcation changed by a constant amount δ per cycle.

Based upon our assumption that $\dot{x}$ is constant, the distance of x from its critical value for bifurcation to quiescence is $\epsilon(t_h - t)$, t_h being the time at which x reaches the homoclinic bifurcation. The "instantaneous" period $T_{hom}(t)$ of the cycles at time t can be expected to have an expansion with leading terms $a_1 \ln(t_h - t) + a_2$. This implies that the times t_n of successive returns to the cross section should satisfy a recursion relation that is approximated by $t_{n+1} = t_n + a_1 \ln(t_h - t_n) + a_2$. From this recursion we want to derive a function that gives the leading asymptotic properties of the periods as a function of t_n. To do so, we compare the solutions of the difference equation with the solutions of the differential equation $\tau' = a_1 \ln(t_h - \tau) + a_2$. Here τ is a new "time-like" variable in terms of which x evolves at a constant rate. The solutions of these two equations have the same leading order asymptotics near t_h that we express in terms of $s = t_h - t$, the time until the transition occurs. Both τ and t_n become unbounded with leading order term $s \ln(s)$. Substituting this leading order term into the asymptotic expansion for the instantaneous periods, we conclude that the dependence of the instantaneous periods on s should behave like

$T_{hom}(s) = c_1 \ln(s^{-1}) + c_2 \ln(\ln(s^{-1})) + c_3$. Here s was defined so that it decreases in constant increments per cycle, $s = 0$ representing the cycle at which the homoclinic transition occurs. The functional form of $T_{hom}(s)$ is predicted to fit plots in which there is one point for each cycle of a tonically firing neuron, the abscissa counting the number of preceding cycles and the ordinate giving the interspike interval of the cycle.

Saddle-node bifurcations and transitions: Consider a frozen system with a single slow variable x having a saddle-node bifurcation at $x = 0$. Assume that there is a family of periodic orbits for $x < 0$ that terminates at the saddle-node bifurcation. The periods of these periodic orbits are unbounded as the bifurcation is approached. At the bifurcation, there is a single trajectory that approaches the new equilibrium as $t \to -\infty$. This trajectory also approaches the degenerate equilibrium as $t \to \infty$, see Figure 1d. In the setting of a neural model, the system is on the edge of excitability: any depolarization, however slight, will induce the system to fire an action potential and then return to quiescence. For parameters close to the bifurcation parameter for the family of periodic orbits, the flow in phase space past the location where the equilibrium emerges slows and the period of the periodic orbits grows. Near the bifurcation, the evolution of the vector field along the periodic orbits is approximated by solutions of the equation $\dot{y} = -x + y^2$ with $x < 0$ proportional to the distance of the parameter from its bifurcation value (Guckenheimer and Holmes, 1993). The time that it takes a trajectory to pass through a fixed neighborhood of the origin is proportional to $(-x)^{1/2}$. This can be seen by rescaling the equation by setting $y = (-x)^{1/2}Y$ and $T = (-x)^{1/2}t$ to obtain $Y' = 1 + Y^2$ and observing that solutions of this equation go from $-\infty$ to ∞ in finite time. Thus, the functional form of interspike intervals are predicted to fit a function of the form $I_{sn} = c_1 + c_2(-x)^{-1/2}$. The term c_1 in I_{sn} accounts for the time required for the periodic orbit to return to the neighborhood of the emerging equilibrium when it escapes from this region.

If we now let $\epsilon > 0$ and consider slow evolution of x satisfying $\dot{x} = \epsilon$, the saddle-node transition can be analyzed in a heuristic manner sim-
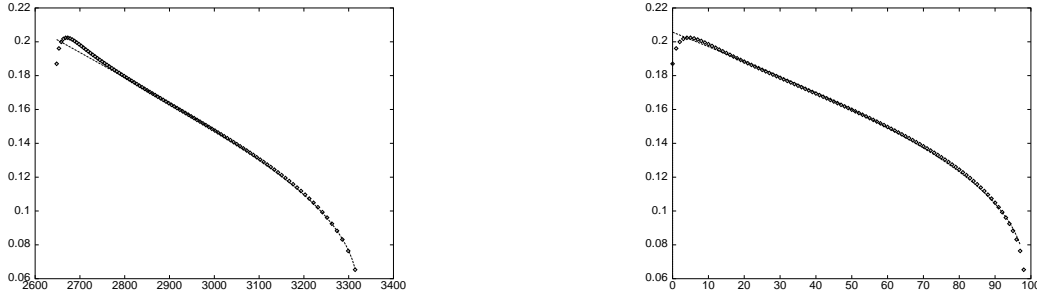
Fig. 2. Reciprocals of interspike intervals from a trajectory in the Morris-Lecar model that undergoes homoclinic bifurcation. In the left diagram, the horizontal axis is time along the trajectory at the end of each period. In the right diagram, the horizontal axis is spike number. The data have been fit with curves of logarithmic type from Table 4.

ilar to our analysis of homoclinic transitions. As in the homoclinic case, we observe here oscillations with growing period, but the quantitative rate of growth is different. The periods of successive cycles grow as $s^{-1/2}$ with $s = t_{sn} - t$ the time prior to the time t_{sn} at which transition occurs. Note that s is a decreasing function. We can also express the asymptotic growth of the periods in terms of cycle number. Set t_n to be the time of spike n in a sequence. We estimate that $t_{n+1} = t_n + c_1 + c_2(t_{sn} - t_n)^{-1/2}$ based upon our derivation of the function I_{sn} and the assumption that x varies at a constant rate. Regard the cycle number as a discrete value of a continuous variable τ and express s as a function of τ. The difference equation for t_n can then be viewed as a discretization of the differential equation $ds/d\tau = c_1 + c_2(s)^{-1/2}$, obtained by replacing $ds/d\tau$ by $s(n+1) - s(n) = t_{sn} - t_{n+1} - (t_{sn} - t_n) = t_n - t_{n+1}$. We compute that the leading term in the asymptotic expansion of $s(\tau)$ is $\tau^{2/3}$. The asymptotic expansion of the interspike intervals as a function of τ, the number of cycles prior to bifurcation, has leading term $\tau^{-1/3}$. This heuristic argument is consistent with the classical asymptotic analysis of flow past a saddle-node or fold in singularly perturbed systems (Mishchenko 1980). The classical analysis is based partly on rescaling the equation $\dot{x} = -\epsilon t + x^2$ to $X' = -T + X^2$ by setting $x = \epsilon^{1/3}X$ and $T = \epsilon^{1/3}t$. This rescaling indicates that the time required for trajectories to pass through a neighborhood of the origin is proportional to $\epsilon^{-1/3}$. These asymptotics suggest that by the time that the slow parameter declines to a magnitude comparable to $\epsilon^{1/3}$, the subsequent periods of the cycles will be comparable to $\epsilon^{-1/3}$.

The final cycles in the oscillation are likely to be reached when the slow variable declines to a magnitude comparable to $\epsilon^{2/3}$ rather than ϵ.

Test on Morris-Lecar System: To test our heuristic arguments about the properties of interspike intervals during homoclinic and saddle-node transitions, we used a model version of the Morris-Lecar model studied by Rinzel and Ermentrout (1989). This is a three dimensional dynamical system with two fast variables and one slow variable, obtained by adding a slowly varying variable to the Morris-Lecar model for an electrically excitable membrane. The equations defining the model are

$$\dot{w} = 0.5\phi\left(1 + \tanh\left(\frac{v - v_3}{v_4}\right) - w\right)\cosh\left(\frac{v - v_3}{2v_4}\right)$$

$$\dot{v} = -0.5\bar{g}_{Ca}\left(1 + \tanh\left(\frac{v - v_1}{v_2}\right)\right)(v - 1)$$
$$\quad -\bar{g}_K w(v - v_K) - \bar{g}_l(v - v_l) + i$$

$$\dot{i} = \epsilon(v^* - v - \alpha i)$$

The variables v and w in the model represent membrane potential and an activation variable for a voltage gated potassium conductance. The third equation introduces an ad hoc variable i that introduces a current to the membrane that slowly relaxes towards an equilibrium value $(v^* - v)/\alpha$ when v remains constant. The variable i is the slow variable of this system; v and w are the fast variables. The frozen system has $\epsilon = 0$.

We chose a set of parameter values in the modified Morris-Lecar model such that the termination of the active phase occurs via a homoclinic transition. The interspike interval gives a mea-
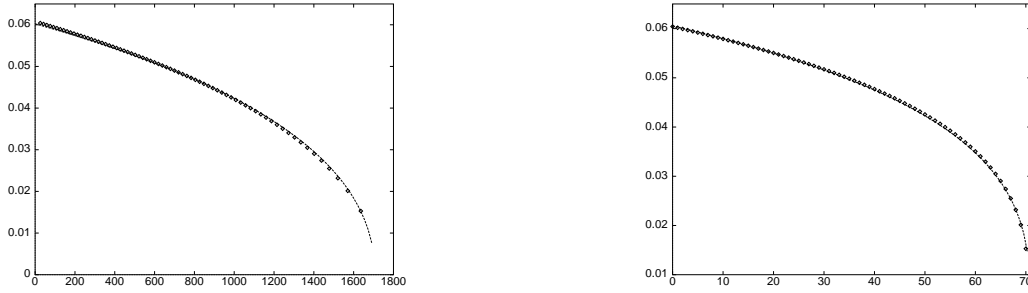
Fig. 3. Reciprocals of interspike intervals from a trajectory in the Morris-Lecar model that undergoes saddle-node in a cycle bifurcation. In the left diagram, the horizontal axis is time along the trajectory at the end of each period. In the right diagram, the horizontal axis is spike number. The data have been fit with curves of square root type from Table 4.

sure of the "instantaneous" period of the oscillations in the model data, and we denote its reciprocal the instantaneous spike frequency. The diamond symbols in Figure 2a plot the instantaneous spike frequency for each cycle as a function of the time at which that interspike interval ends. The dashed curve is a fit of a function $1/(21 - 2.46 \ln(3325 - t))$ of the form $1/(c_1 + c_2 \ln(t_h - t))$ to the data. As predicted by the theory, such a function does an excellent job of matching the "tail" of the data as the frequency of spiking slows and then terminates. The theory that we have developed is only asymptotic and makes no predictions about the period of oscillations long before the termination. In this case, the function fits more than the last half of the data set extremely well, certainly within the variation that would be expected from experimental data. Figure 2b plots the same data for instantaneous spike frequency as a function of cycle number. A function $1/(13.9 - 1.62 \ln(99 - s) - 1.0 \ln(\ln(99 - s)))$ of the form $1/(c_1 + c_2 \ln(N_h - s) + c_3 \ln(\ln(N_h - s)))$ predicted by the theory is fit to the data. As in Figure 2a, the fit of the predicted function to more than the last half of the data is excellent. The optimal fit of the relation predicted by a saddle-node termination is much poorer.

Figure 3 shows comparable data to Figure 2 for a different set of parameter values in which the termination of the active phase of bursting in the modified Morris-Lecar model occurs via a saddle-node transition. The diamond symbols in Figure 3a plot instantaneous spike frequency as a function of the time at which the interspike interval ends, while Figure 3b plots the same data for $1/interspikeinterval$ as a function of cy-

cle number. In Figure 3a, a function $1/(3.6 + 530/\sqrt{1705 - t})$ of the form $1/(c_1 + c_2/\sqrt{t_{sn} - t})$ suggested by the theory is fit to the model data. Here the function predicted by the theory fits the entire data set extraordinarily well, far better than might be expected from the asymptotic nature of the theory. Similarly, in Figure 3b, a function $1/2.1 + 58.85(71 - s)^{-/3}$ of the form $1/(c_1 + c_2(N_{sn} - s)^{-1/3})$ suggested by the theory fits the entire data set extremely well despite the fact that the theory predicts only that such a function will give a good approximation to the data near the termination of spiking. Functions of the form predicted by a homoclinic termination give a poor fit to this data. These tests with data from the modified Morris-Lecar model confirm that the validity of our asymptotic theory for distinguishing homoclinic and saddle-node transitions at the end of a period of spiking.

3. Model Studies

To further explore the properties associated with the termination of spiking in a system undergoing spike frequency adaptation, we performed additional investigations on a more realistic single-compartment conductance based model for a neuron that we have studied experimentally, the LP cell of the stomatogastric ganglion of *Panulirus interruptus.* Our starting point is a model we have used to explore mechanisms for postinhibitory rebound in the LP neuron (Harris-Warrick et al. 1995). This model is a modification of one generated by Buchholtz et al. (1992) based upon voltage clamp measurements of Golowasch et al. (1991). We added to this model a very slowly ac-

Table 1: Mathematical model of the LP neuron

$$
\begin{aligned}
C_m \dot{v} \;=\; & -(\underbrace{\bar{g}_{Na}\, m_\infty^3\, h\, (v - E_{Na})}_{I_{Na}}) + (\underbrace{\bar{g}_{Ca1}\, a_{Ca1}\, b_{Ca1} + \bar{g}_{Ca2}\, a_{Ca2})\, (v - E_{Ca})}_{I_{Ca}} \\
& + \underbrace{\bar{g}_K\, n^4 (v - E_K)}_{i_{K(V)}} + \underbrace{\bar{g}_{K(Ca)}\, a_{K(Ca)}\, b_{K(Ca)}\, (v - E_K)}_{I_{K(Ca)}} \\
& + \underbrace{(\bar{g}_{Af}\, b_{Af} + \bar{g}_{As}\, b_{As})\, a_A^3\, (v - E_K)}_{I_A} + \underbrace{\bar{g}_h\, a_h\, (v - E_h)}_{I_h} \\
& + \underbrace{\bar{g}_s\, a_s\, (v - E_k)}_{I_s} + \underbrace{\bar{g}_l\, (v - E_l)}_{I_l}) + I_{ext}
\end{aligned}
$$

$$
I_{Na} :
\begin{cases}
m_\infty \;=\; \left(1 + 15\, e^{-(v+34)/13\, \frac{(1 - e^{-(v+6)/20})}{0.11(v+6)}}\right)^{-1} \\[2mm]
\dot{h} \;=\; 500 \left(0.08(1-h)e^{-(v+39)/8} - \frac{h}{1 + e^{-(v+40)/5}}\right)
\end{cases}
$$

$$
I_{Ca} :
\begin{cases}
\dot{Ca} \;=\; -300\, (\bar{g}_{Ca1}\, a_{Ca1}\, b_{Ca1} + \bar{g}_{Ca2}\, a_{Ca2})\, (v - E_{Ca}) + 360\,(0.05 - Ca) \\[2mm]
\dot{a}_{Ca1} \;=\; 50 \left(\left(1 + e^{-(v+11)/7}\right)^{-1} - a_{Ca1}\right) \\[2mm]
\dot{a}_{Ca2} \;=\; 10 \left(\left(1 + e^{-(v-22)/7}\right)^{-1} - a_{Ca2}\right) \\[2mm]
\dot{b}_{Ca1} \;=\; 16 \left(\left(1 + e^{(v+50)/8}\right)^{-1} - b_{Ca1}\right)
\end{cases}
$$

$$
i_{K(V)} :
\left\{ \dot{n} \;=\; 282 \left(1 + e^{-(v-10)/22}\right)^{-1} \left(\left(1 + e^{-(v+25)/17}\right)^{-1} - n\right) \right.
$$

$$
I_{K(Ca)} :
\begin{cases}
\dot{a}_{K(Ca)} \;=\; 45 \left(\frac{Ca}{(1 + e^{-(v+20+0.6Ca)/23})(1 + e^{-(v+23+0.6Ca)/6})(2.5 + Ca)} - a_{K(Ca)}\right) \\[2mm]
\dot{b}_{K(Ca)} \;=\; 35 \left(\frac{0.6}{0.6 + Ca} - b_{K(Ca)}\right)
\end{cases}
$$

$$
I_A :
\begin{cases}
\dot{a}_A \;=\; 140 \left(\left(1 + e^{-(v+32)/16}\right)^{-1} - a_A\right) \\[2mm]
\dot{b}_{Af} \;=\; 30 \left(\left(1 + e^{(v+75)/12}\right)^{-1} - b_{Af}\right) \\[2mm]
\dot{b}_{As} \;=\; 10 \left(\left(1 + e^{(v+75)/12}\right)^{-1} - b_{As}\right)
\end{cases}
$$

$$
I_h :
\left\{ \dot{a}_h \;=\; 0.1 \left(1 + e^{-(v+100)/13}\right) \left(\left(1 + e^{(v+110)/12}\right)^{-1} - a_h\right) \right.
$$

$$
I_s :
\left\{ \dot{a}_s \;=\; 0.0985 \left(\left(1 + e^{-(v-v_s)/4}\right)^{-1} - a_s\right) \right.
$$

Table 2: Fixed parameters for model of the LP neuron

Parameter	Value	Meaning	Units
$\bar{g}_{Af}$	1.5	fast A current conductance	μS
$\bar{g}_{As}$	1.3	slow A current conductance	μS
$\bar{g}_{K(Ca)}$	5	K(Ca) current conductance	μS
$\bar{g}_l$	0.05	leak current conductance	μS
$\bar{g}_h$	0.1	sag current conductance	μS
E_K	-86	Potassium reversal potential	mV
E_l	-52	leak reversal potential	mV
E_h	-10	sag reversal potential	mV
E_{Ca}	140	Ca reversal potential	mV
E_{Na}	50	Sodium reversal potential	mV
C_m	0.002	Membrane capacitance	nF

tivating, non-inactivating current that is an idealization of an outward potassium current with simple kinetics. The time constant for the activation was set to slow current $0.0985s^{-1}$, and the equilibrium value for its activation is a sigmoidal function centered at -42 mv. The equations for the model and the fixed parameters are given in Tables 1 and 2.

We analyzed this model in two forms, the singularly perturbed system (as given in Tables 1

Fig. 4. Equilibrium and bifurcation curves for the frozen LP model with the parameter values of column A of Table 3. The six solid lines are curves of equilibria for $I_{ext} = 0 \dots 5$ nA moving from left to right. The dashed line is the curve of saddle-node bifurcation points which passes through the vertical tangency of each of the equilibrium curves. The dotted line is a curve of Hopf bifurcation points. The Hopf and saddle-node curves intersect near $I_{ext} = 4$ nA at a codimension two bifurcation. The equilibrium points below both the saddle-node and Hopf curves are stable, whereas the others are unstable.

and 2) and the frozen system. The frozen system corresponds to eliminating the equation for slow current activation $\dot{a}_s$ in Table 1 and then setting $a_s \equiv 1$ corresponding to full activation of the slow outward potassium current in the voltage equation. We first studied how the eigenvalues of equilibrium solutions of the frozen system varied with the parameters $\bar{g}_s$, the maximal conductance of the slow current, and I_{ext}, the externally applied current. Within the parameter regimes in which we looked, the singularly perturbed system exhibits three different mechanisms for spike termination. The first is a saddle-node of equilibria interrupting a limit cycle, the second is a homoclinic bifurcation and the third is a more complicated subcritical Hopf bifurcation mechanism that we discuss below.
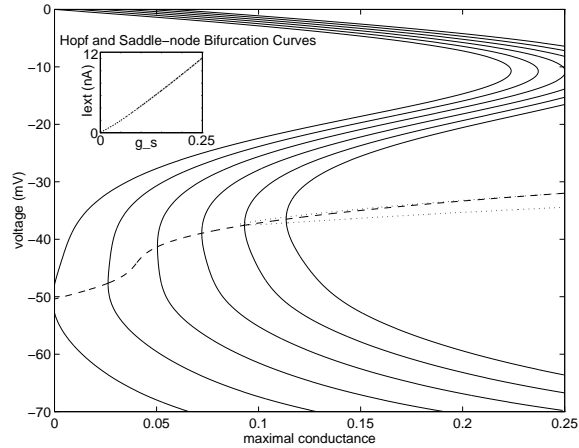
The Frozen System: The LP model has a linear dependence upon many of its parameters, for example, the maximal conductance parameters. If one of these parameters is allowed to vary and the remaining parameters are held fixed, the frozen system model has exactly one equilibrium point for each value of the voltage, v_0. Furthermore, the equilibrium v_0 remains fixed along a line in the $(I_{ext}, \bar{g}_s)$ parameter plane. For a fixed value of I_{ext} the equilibrium points in the $(\bar{g}_s, v)$-plane form an S-shaped curve as depicted in Figure 4. For each point in the $(\bar{g}_s, v)$-plane there is exactly one value of I_{ext} that creates an equilibrium at this point of the $(\bar{g}_s, v)$-plane. The six S-shaped curves in Figure 4 are the curves of equilibrium

Table 3: Varying parameters for model of the LP neuron

Parameter	A	B	C	D	Meaning	Units
$\bar{g}_K$	0.1	0.7	1.3	0.4	K current conductance	μS
$\bar{g}_{Ca1}$	0.21	0.0001	0.0001	0.21	Inactivating Ca current conductance	μS
$\bar{g}_{Ca2}$	0.047	0	0	0.047	Noninactivating Ca current conductance	μS
$\bar{g}_{Na}$	2700	2300	1900	2700	Na current conductance	μS
$\bar{g}_s$	0.15	0.15	0.15	0.1	slow K current conductance	μS
v_s	-42	-42	-42	-41	slow K current half activation	mV

points for $I_{ext} = 0, 1, \ldots, 5$ nA, moving from left to right. The left folds of the equilibrium curves i.e., the points of the equilibrium curves with tangent parallel to the v axis, are saddle-node bifurcations which give birth to two new fixed points with varying g_s. For values of g_s smaller than the value at the fold, there are no nearby equilibria, while for values of g_s larger than the value at the fold, there are two nearby equilibria. At the fold point, the equilibrium point has a single zero eigenvalue. The remaining eigenvalues either all have negative real parts, or there is a single pair of complex eigenvalues with positive real part. The equilibrium points that are above the left fold; i.e., more depolarized, are always unstable points with either a one or three dimensional unstable manifold while those on the lower branch are either stable, or unstable with a two dimensional unstable manifold. For values of $\bar{g}_s$ to the left of the saddle-node bifurcation, the system is in a tonic firing state. However, the behavior of the system for values of $\bar{g}_s$ to the right of the saddle-node bifurcation can take several forms depending on the system parameters. Results for the three sets of parameter values given in Table 3 are discussed below.

The parameter values in column A of Table 3 are our "base" values, representing nominal control conditions for the neuron, Figure 4 gives additional information about the bifurcations of the frozen system. In the $(\bar{g}_s, I_{ext})$-plane there is a curve of saddle-node bifurcations. Its projection into the $(\bar{g}_s, v)$-plane is the curve in Figure 4 that passes through the fold points on the left sides of the equilibrium curves. The U-shaped curve opening to the right on the diagram is the projection of a curve of Hopf bifurcation points that occur with varying $(\bar{g}_s, I_{ext})$. There is a codimension

two bifurcation where the saddle-node curve and the Hopf curve intersect. This is a new feature that does not occur in the Morris-Lecar system, since the fast Morris-Lecar subsystem is only two dimensional and this codimension two bifurcation requires a three dimensional phase space. At the codimension two point, the equilibrium point has one zero eigenvalue and a pair of pure imaginary eigenvalues. We shall denote as I_c the value of I_{ext} at which this codimension two bifurcation occurs (for the Table 3, column A parameter values, I_c is approximately 4 nA). For $I_{ext} < I_c$, the saddle-node bifurcation occurs on the limit cycle and all the equilibria on the lower branch are globally attracting, so that as $\bar{g}_s$ is increased past the saddle-node, the system moves from a state of tonic firing to a quiescent state in which all initial conditions lead to the quiescent state, perhaps after firing a single potential. Approaching the bifurcation, the period of firing of the limit cycle increases without bound as described above with the theory of saddle-node bifurcations. For $I_{ext} > I_c$, the new equilibrium point created at the saddle-node bifurcation appears nearby, but off the limit cycle, and has, in addition to the one dimensional center manifold, a two dimensional unstable manifold which does not disappear until the Hopf bifurcation is reached. As a result, the limit cycle representing tonic firing persists past the saddle-node bifurcation as $\bar{g}_s$ is increased. The mechanism associated with the termination of firing in this parameter region does not fit the cases analyzed in the previous section, but appears to be related to the codimension two bifurcation occurring at I_c.

Although Hopf bifurcation produces a family of periodic orbits, the stable limit cycle that we see to the left of the Hopf point does not shrink directly to the Hopf point. Instead, it appears that
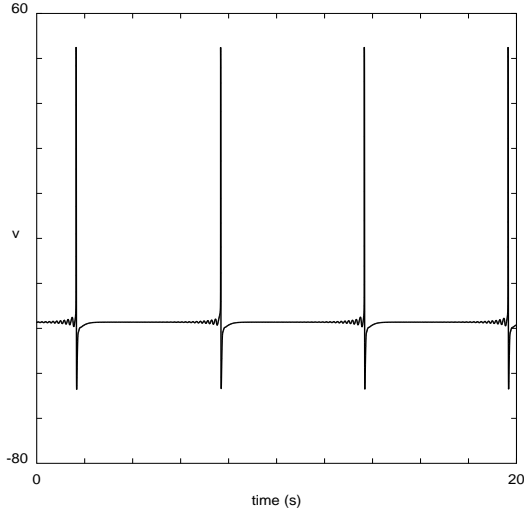
Fig. 5. Equilibrium and bifurcation curves for the frozen LP model with the parameter values of column C of Table 3. The six solid lines are curves of equilibria for $I_{ext} = 0 \ldots 5$ nA moving from left to right. There are no saddle-node bifurcations in this parameter regime but Hopf bifurcation curve (dotted line) separates the stable equilibria (below) from the unstable equilibria (above).
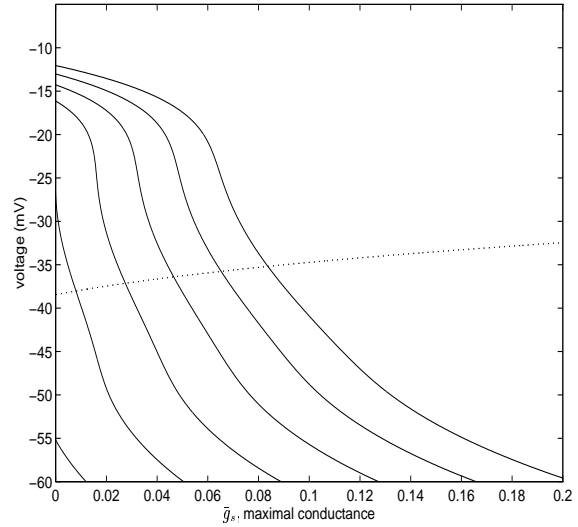

Fig. 6. A trajectory from the frozen LP model that comes close to an equilibrium undergoing Hopf bifurcation. Each spike is preceded by growing subthreshold oscillations preceding each spike. Computation of a cross-section for this trajectory (not shown) suggests that the trajectory is chaotic.

the Hopf bifurcation is subcritical, giving rise to a small, finite period, unstable limit cycle to the right of the bifurcation. Thus the death of our stable limit cycle as the Hopf point is approached from the left is occurring by some process different from the Hopf mechanism. Within the narrow region to the right of the saddle-node but left of the Hopf bifurcation, the equilibrium points on the lower branch have a complex pair of eigenvalues with positive real part. As the parameter $\bar{g}_s$ increases past the saddle-node bifurcation into this region, no abrupt change is noticed in the limit cycles. However, as $\bar{g}_s$ continues to increase toward the Hopf bifurcation, fast, low-amplitude growing oscillations become evident during the rebound phase of the spike. Simultaneously, the spiking frequency continues to decrease. Figure 5 shows a simulated voltage trace for this low frequency spiking.

Very near the Hopf point, the limit cycle has an extremely long period where most of its time is spent near the unstable equilibrium oscillating at a constant high frequency, but with slowly increasing amplitude. The cell stays in this state of slowly growing fast oscillations until their ampli-

tude becomes large enough to push the cell above threshold, eliciting a single action potential and a subsequent return very close to the equilibrium point to continue the process again. The growth and frequency of the underlying fast oscillations correspond to what one would expect from the real and imaginary parts of the complex eigenvalues. The length of the period of the limit cycle seems to be determined primarily by the growth rate away from the equilibrium, that is, by the real part of the complex eigenvalue. This state appears to be very close to a homoclinic orbit of focal type; i.e., the homoclinic orbit approaches the equilibrium from the direction of a real, negative eigenvalue and escapes from the vicinity of the equilibrium in the directions of a pair of complex eigenvalues. However, analysis of homoclinic orbits that occur sufficiently close to a subcritical Hopf bifurcation suggests that there may be chaotic attractors to the system in this parameter regime. To explore this possibility, we computed a cross-section obtained from a trajectory undergoing repeated cycles of small amplitude, fast oscillations near the equilibrium followed by a single action potential. The parameter values for this trajectory were lo-
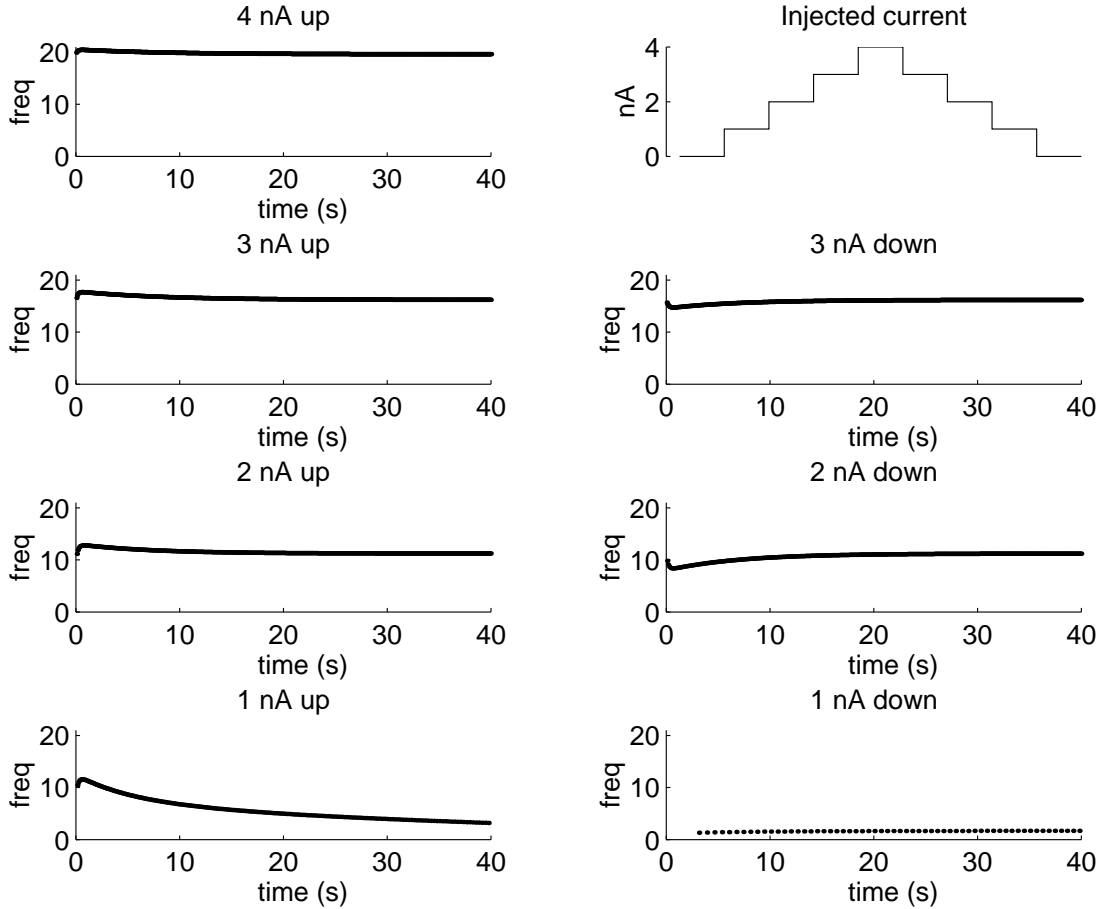
Fig. 7. Spike frequency adaptation for the LP cell model with the parameter values of column D of Table 3. The graphs on the left are for the upward portion of the protocol, while those on the right are for the downward portion. The protocol is illustrated in the top right panel. Injected current increases by 1 nA from bottom to top on the left and decreases by 1 nA from top to bottom on the right.

cated to the left of the Hopf bifurcation point for $I_{ext} > I_c$. Points of the cross-section did not converge to a fixed point as they would if the trajectory was periodic, but continued to wander along a curve. Details of the successive oscillations of the model neuron varied in an apparently chaotic fashion for the chosen parameter values. Glendinning and Sparrow (1984) have shown that the approach to a homoclinic orbit of focal type may be accompanied by sequences of saddle-nodes of limit cycle and period-doubling bifurcations of a periodic orbit together with chaotic attractors that are formed and then lose stability. We conjecture that similar complex dynamics are occurring here in our model of the LP cell. The asymptotic analysis of periods of periodic orbits in this regime is

problematic since we are unsure of the parameter domains in which stable periodic orbits exist. Moreover, there are two competing factors for determining the time required for trajectories passing near the equilibrium to escape: namely, the magnitude of the real part of the unstable eigenvalue and the distance of closest approach to the equilibrium.

We made two sets of parameter modifications that are outside the normal biological range of parameters for the purpose of testing the mathematical theory of the previous section. The parameter values in column B of Table 3 differ from those of column A in that there is a virtually complete removal of the calcium currents, a small reduction of the sodium conductance and a substantial increase
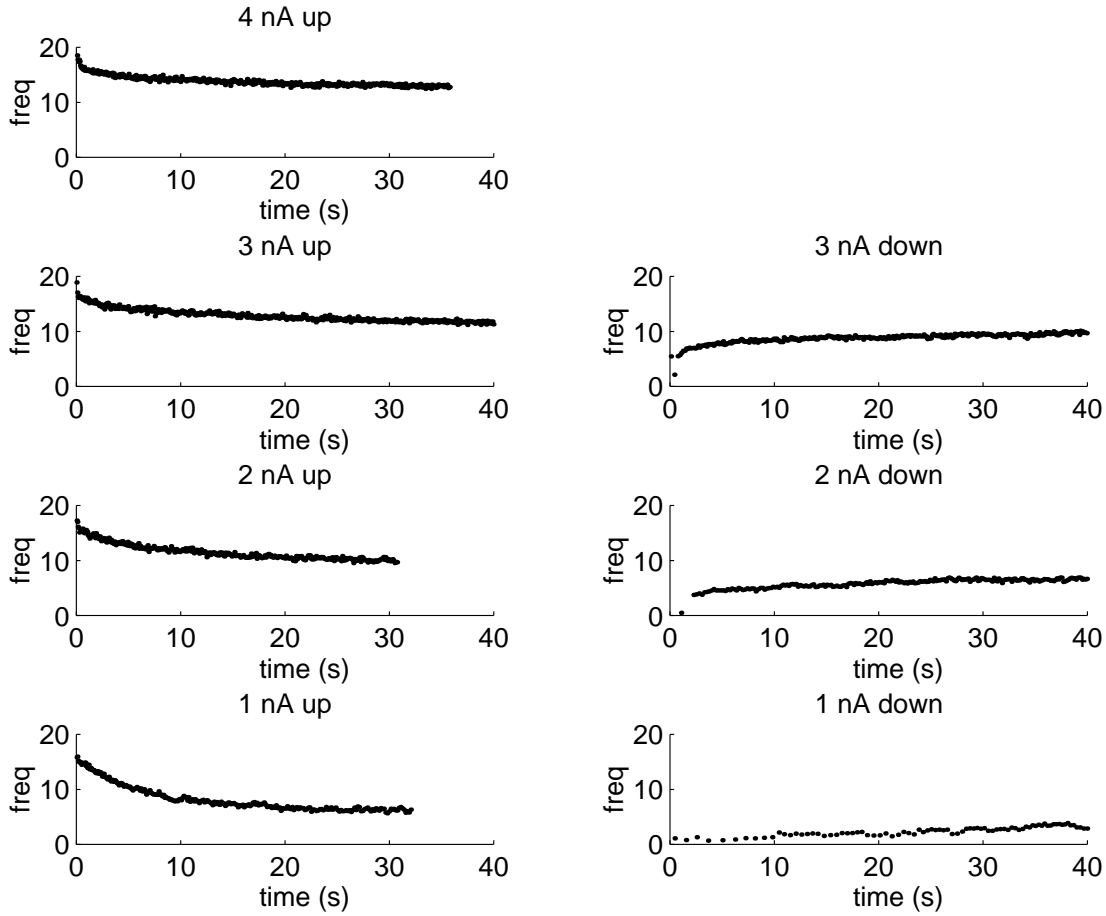
Fig. 10. Spike frequency adaptation from an experiment on the LP cell. The graphs on the left are for the upward portion of the protocol, while those on the right are for the downward portion. Injected current increases by 1 nA from bottom to top on the left and decreases by 1 nA from top to bottom on the right.

in the delayed rectifier conductance. While the bifurcation diagram looks qualitatively the same as Figure 4 for the parameter values in column B of Table 3, homoclinic bifurcation occur at the termination of spiking for $I_{ext} < I_c$ with variations in $\bar{g}_s$. The mechanism for spike termination for $I_{ext} > I_c$ is the same as the complex scenario described above. For $I_{ext} < I_c$, as $\bar{g}_s$ is increased, the saddle-node bifurcation gives birth to two equilibria near the limit cycle, the lower one of which is stable but not globally attracting, while the one dimensional unstable manifold of the upper one winds tightly around the limit cycle representing tonic spiking. Thus the model cell displays bistability in this region to the right of the saddle-node bifurcation. As $\bar{g}_s$ is increased slightly more, the unstable manifold of the saddle and the limit cycle

coalesce in a homoclinic loop after which the stable equilibrium becomes globally attracting and the system becomes excitable, but quiescent.

A further reduction of the sodium conductance and an increase in the delayed rectifier conductance gives the parameter values in column C of Table 3. For these parameter values, the bifurcation diagram is shown in Figure 6.

Here the equilibrium curves have lost their S-shape and do not have a vertical tangent at any point within the parameter regime of interest. This means that there is exactly one equilibrium point for each value of $\bar{g}_s$ and no saddle-node bifurcations occur. The curve of Hopf bifurcation points is still present dividing the stable equilibria to the bottom from the unstable equilibria to the top. Termination of the limit cycle occurs via
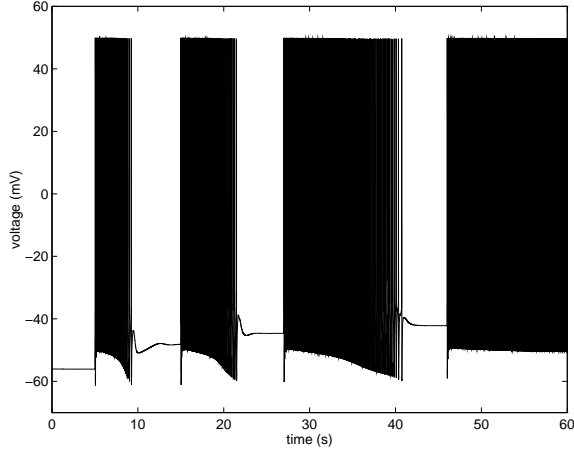
Fig. 8. Voltage trace from the LP cell model with the parameter values of column A of Table 3. The injected current is increased from 0 to 4 nA in 1 nA increments. Each increase in the injected current begins a new phase of activity. For the first three steps, the frequency of the action potentials slowly decreases to zero and the voltage settles to a new equilibrium value. For $I_{ext} = 4$ nA, the model remains in a tonic firing state.

the subcritical Hopf bifurcation mechanism as $\bar{g}_s$ is increased past the Hopf point.

Time Dependent Activation of the Slow Current When activation of the slow current is added to the model, the slow increase in a_s over time (with $\bar{g}_s$ held constant) mimics the increase of $\bar{g}_s$ described above for the frozen system. The time constant, k_s, for the activation variable was set to 0.0985 s^{-1}, based on estimates of slow spike adaptation from experimental data obtained during depolarization of an LP neuron (Peck, unpublished). For many of our computer simulations and experiments on the real LP cell, we followed a "stair step" current injection protocol: an external injected current was first increased by 1 nA steps to a maximum of 4 or 5 nA and then decreased by 1 nA steps back to zero. The applied current was held steady for about a half a minute between steps to allow the cell to settle to either a resting state or a tonically firing state with constant firing frequency.
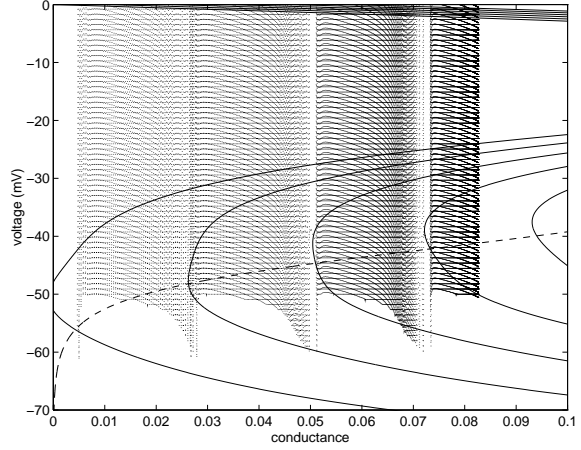

Fig. 9. The same voltage trace as in Figure 9 plotted as a function of the conductance of the slow current. The voltage trace is plotted as a dotted line in order to be able to see the other curves on the graph. (The apparent horizontal and curved lines within the voltage trace are an artifact of the spacing of the dots in the closely packed vertical lines.) The solid lines are the equilibrium curves as in Figure 4. The dashed line is the null cline for the conductance of the slow current. Note how for each value of I_{ext} the activity continues until the saddle-node bifurcation is reached after which the solution settles to the point at the intersection of the equilibrium curve and the null cline. For $I_{ext} = 4$ nA, the conductance fails to increase far enough to reach the saddle-node bifurcation and thus the system remains in a tonic firing state.

We wished to determine if the model could adequately capture the LP cell behavior in cases where the cell underwent spike frequency adaptation but not termination. From Figure 4 we see that the spike terminating bifurcations occur when the conductance of the slow potassium current becomes large. Thus, these bifurcations are never reached if the conductance of the slow current is sufficiently small. The parameters in column D of Table 3 differ from those in column A in that the slow current half activation is shifted to a more depolarized value and the maximal conductance is lowered, both of which cause a reduction in the slow current. The spike frequency data for a stair step current injection simulation is shown in Figure 7. Note that during the upward part of the injection staircase, after an increment in the external current, the spike frequency decreases slowly to a steady value. The amount of change is less and the final steady value is higher for higher values of the external current. During the downward portion of the staircase, the spike frequency rises
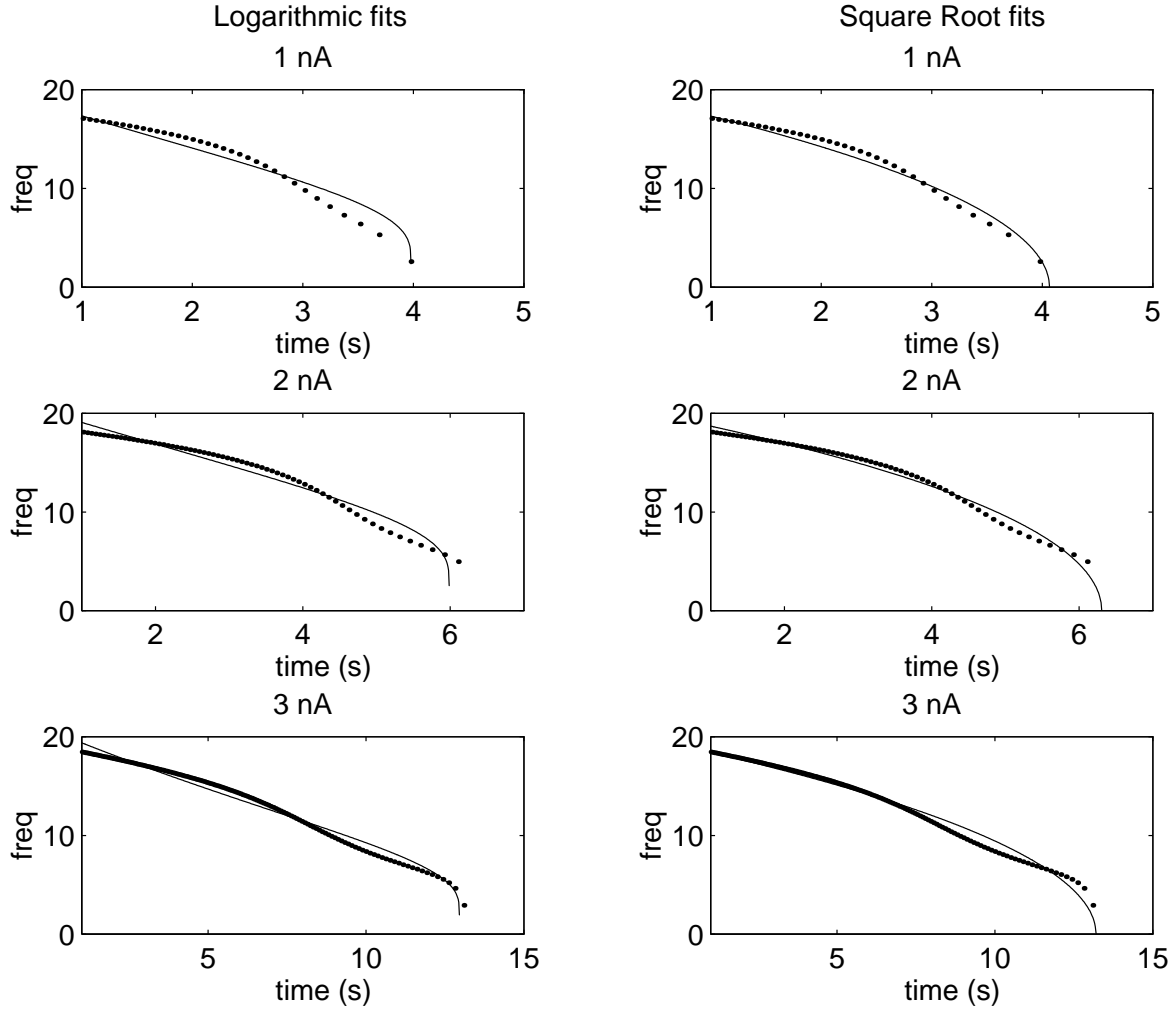
Fig. 11. Instantaneous frequency data from the LP cell model for the parameter values in column A of Table 3. The same data is plotted in both the left and right columns. Optimal least squares fits to the logarithmic and square root functions of Table 4 are overlaid on the data points in the left and right columns respectively. The sum of the norm of the residuals divided by the number of data points for each pair of fits are as follows. (The first value is for the logarithmic fit and the second for the square root fit.) 1 nA: 0.1280, 0.0867; 2 nA: 0.0701, 0.0579; 3 nA: 0.0418, 0.0414.

after each step to approximately the same steady value as was achieved on the way up. This figure should be compared with Figure 8 which shows real LP cell data from an experiment with a similar current injection protocol. The model and experimental data both display spike frequency adaptation with frequency increasing in response to depolarizing steps and decreasing in response to hyperpolarizing steps.

We next wished to investigate the model behavior in cases where spike termination occurred. Starting from appropriate initial conditions, the

system evolves from a state of tonic firing through a transition to a quiescent state. Figure 9 shows several such events where, after each return to a quiescent state, the externally applied current is stepped up 1 nA. Sudden increases in I_{ext} translate the bifurcation curve to the right so that the system lies in a state to the left of the saddle-node bifurcation curve for the frozen system, that is, in a tonic firing state. Over time, the activation of the slow current increases until either the average voltage during the firing state is not sufficiently large to drive a further increase of the ac-
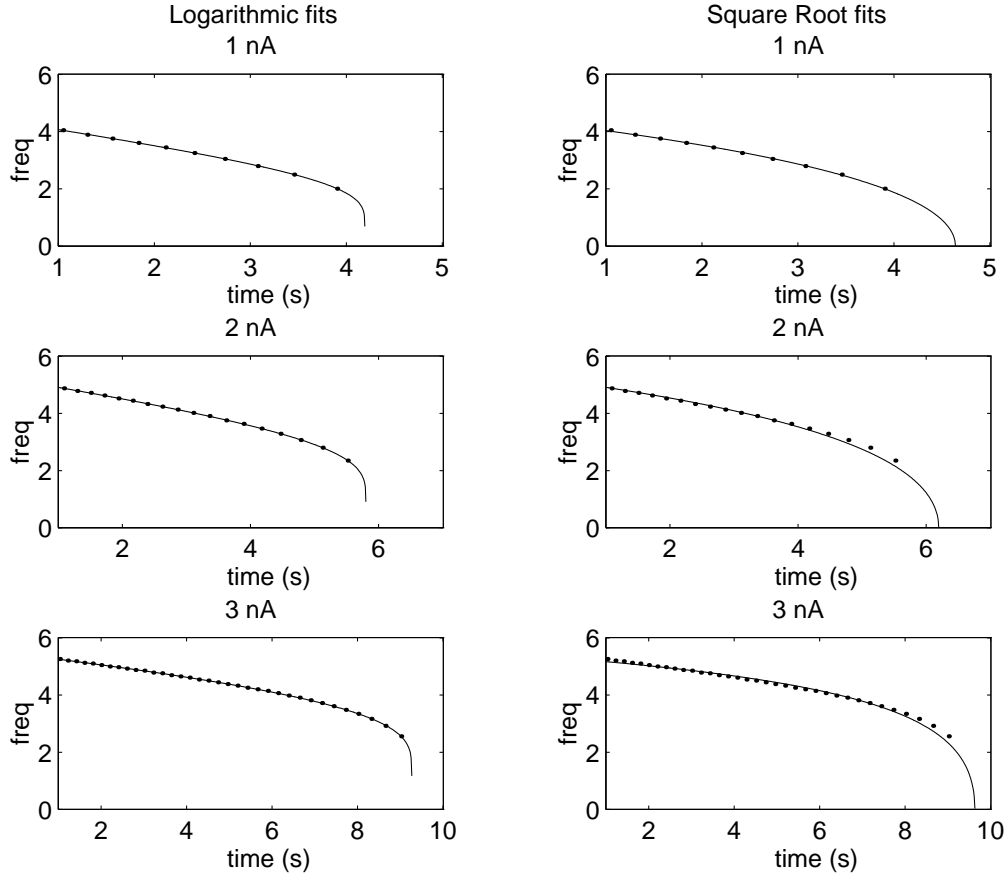
Fig. 12. Instantaneous frequency data from the LP cell model for the parameter values in column B of Table 3. The same data is plotted in both the left and right columns. Optimal least squares fits to the logarithmic and square root functions of Table 4 are overlaid on the data points in the left and right columns respectively. The sum of the norm of the residuals divided by the number of data points for each pair of fits are as follows. (The first value is for the logarithmic fit and the second for the square root fit.) 1 nA: 0.00212, 0.00484; 2 nA: 0.00154, 0.01852; 3 nA: 0.00141, 0.01264.

tivation of the slow current or a spike-terminating transition occurs and the system becomes quiescent once more. Figure 10 shows the same trace as in Figure 9 this time plotted as a function of the conductance, $\bar{g}_s a_s$, rather than time. Overlaid on this trace are the equilibrium curves for the frozen system and the null cline for the variable a_s. This figure illustrates that the system switches from a tonic firing state to a quiescent state as the saddle-node bifurcation is passed. After passing the saddle-node bifurcation, the system tracks the slow manifold i.e., the curve of equilibrium points for the frozen system, until it reaches equilibrium on the null cline for a_s. Once reaching this state,

the externally applied current is increased by 1 nA and the process continues.

Note that the slow variable a_s in this model does not have a constant velocity since its equation of motion is voltage dependent. In particular, we noted distinct increases in the velocity of a_s when approaching a spike terminating transition. This effect is due to the fact that the system tends to remain for long times close to the place where the equilibrium point is about to appear, and the value of the voltage there is more depolarized than the time averaged voltage of the tonic firing state. The net result is that the model accelerates toward the spike termination bifurcation, that is, the frequency of firing drops slightly faster

than would be the case if the slow variable a_s had a constant velocity. However, we can still distinguish homoclinic and saddle-node bifurcations by fitting the frequency data to the asymptotic curves as developed in the previous section. The data for several terminating traces for the parameter values in columns A and B of Table 3 are shown in Figure 11 and 12 respectively. In all of these, $I_{ext} < I_c$ so that the mechanism of termination is either the saddle-node interrupting a limit cycle or a homoclinic bifurcation. As seen in both of these figures, the square root function consistently gives the best fit for the saddle-node case while the logarithmic function performs best for the homoclinic case, as expected. The curves in these figures are of the functional form given in Table 4. They were fit to the data using a nonlinear least squares algorithm with a weighted factor that was set so that the curve reached a frequency of zero within one cycle of the last spike before termination. The sum of the norm of the residuals divided by the number of data points is given in the captions for Figures 11 and 12 for each of the curve fits.

For $I_{ext} > I_c$ with the parameter values in columns A and B of Table 3, the distance between the saddle-node and Hopf bifurcations corresponds to such a small increase in a_s that the region between these two bifurcations is traversed quite quickly, in just a fraction of a single cycle, rendering the effects of the Hopf bifurcation unobservable. However, for the parameter values in column C of Table 3, the spike termination through the subcritical Hopf is readily observable. Instantaneous frequency data for several terminating traces for these parameter values are shown in Figure 13, where, not surprisingly, it is clear that neither the square root function nor the logarithmic function provide a satisfactory fit. Since the exponential growth away from the equilibrium is given by $e^{\lambda t}$, where λ is the real part of the complex unstable eigenvalue, it is reasonable to assume that the period of the limit cycle is dominated by a term proportional to $1/\lambda$. As λ varies nearly linearly with the conductance, which in turn is assumed to vary linearly in time, we suspect that the instantaneous frequency should behave as $A + 1/(B - Ct)$. A fit of the model data to this fractional linear function is shown if Figure 13

where it is seen that the results are significantly better than the fits to square root or logarithmic functions of Table 4.

We comment on one additional feature of the data in Figure 13; namely, the apparent "steps" in the frequency of successive oscillations. There are sudden large drops in the frequency, and the tread of each step is slightly concave downward. A potential explanation for these steps is the presence in the frozen system of regions of multistability in which there are oscillations that make differing number of oscillations surrounding the equilibrium in the direction of the unstable complex eigenvalues. If each of the branches of stable oscillations terminate in a saddle-node of limit cycles, then we expect that the singularly perturbed system will make abrupt transitions among the different stable oscillations. As noted above, such behavior occurs near homoclinic orbits of focal type (Glendinning and Sparrow 1984).

4. Spike Frequency Adaptation in the Stomatogastric Ganglion

We conducted experiments on the LP neuron from California spiny lobsters, *Panulirus interruptus*, obtained from Marinus Inc., Los Angeles, or from Don Tomlinson (San Diego). All drugs and salts were obtained from Sigma Chemical Co. The stomatogastric ganglion was dissected from the animal and prepared for the experiments as described in Selverston et al. (1976). LP cells were isolated from all detectable synaptic input as described by Flamm and Harris-Warrick (1986). Following isolation, a LP neuron was impaled with two microelectrodes, one for current injection and one for voltage recording. In between current injection protocols, the cell was held at a constant membrane potential of -55 mV during the entire experiment; this is similar to the normal resting potential of this neuron under control conditions.

Using the asymptotic analysis described above, we sought to identify the dynamical mechanisms associated with the slowing and termination of firing in the LP neuron. Current was injected into the isolated neuron in the stairstep protocol described above to depolarize the cell and induce it to start firing action potentials. During current pulses of constant magnitude, spike frequency
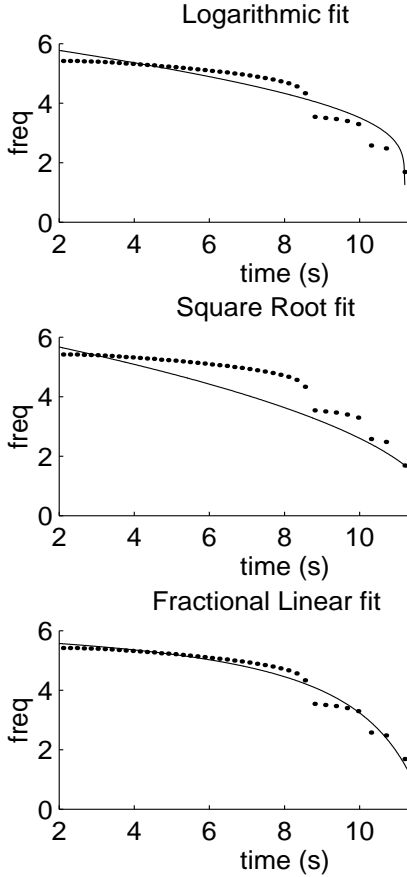
Fig. 13. Instantaneous frequency data from model for the parameter values in column C of $I_{ext} = 4$ nA. Optimal least squares fits for the square root and fractional linear functions ol overlaid on the data points in the three grap of the norm of the residuals divided by the number of data points for each fit is as follows. logarithmic: 0.0436; square root: 0.0923; fractional linear: 0.0265.
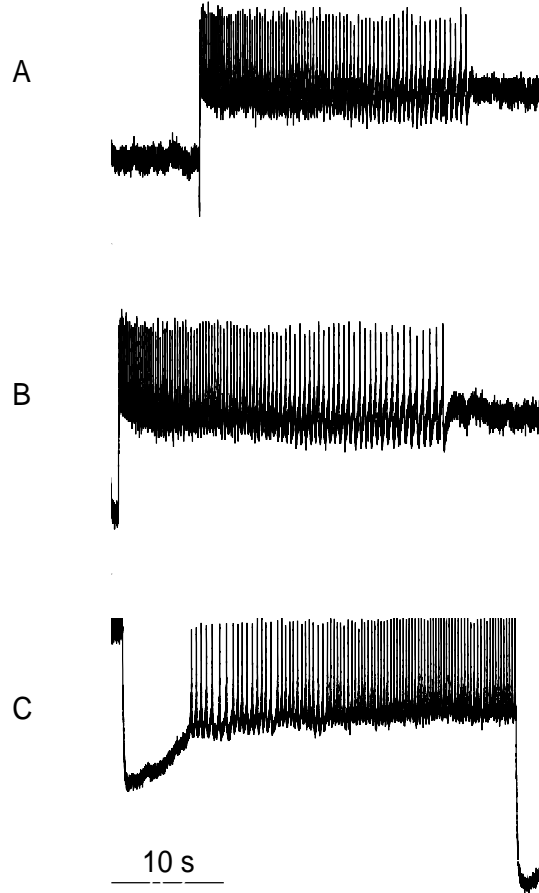

Fig. 14. Voltage recordings from the LP cell showing spike frequency adaptation. In A and B the injected current is increased by 1 nA near the beginning of the trace and then held constant, while in C it is decreased by 1 nA

adaptation occurred, and with low amplitude current injection the firing eventually ceased. The depolarizing current injection was maintained long enough for the firing to cease or for the firing rate to approach an apparent asymptotic value. From voltage recordings of these experiments, we computed the lengths of successive interspike intervals and constructed optimal least square fits of functions of the forms given in Table 4 to their instantaneous spike frequency. Figure 14 shows voltage recordings from three of these experiments, two of which are traces that shut down after a 1 nA step increase in the injected current and one which

shows an increase in firing rate as a result of a 1 nA step decrease in the injected current. Interspike intervals are measured as the time from the preceding action potential to the current action potential.

The LP neuron seems to exhibit an intermediate-time process of adaptation over the first few seconds after the step current injection that is not described in the model. Since we are interested in studying the long-time behavior of the slowly activated adapting current, we eliminated the first two or three seconds of data after each current step from the current-clamp experiments. Data for four typical terminating traces
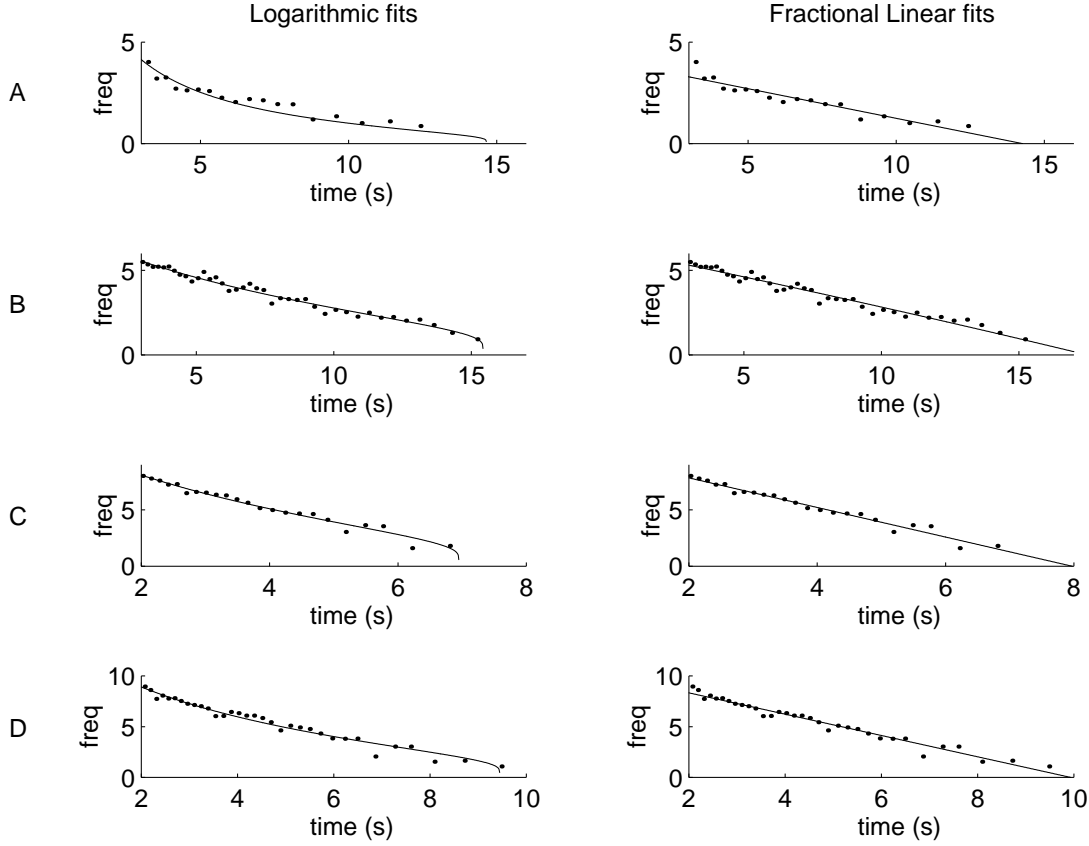
Fig. 15. Instantaneous frequency data from experiments on the LP cell. The same data is plotted in both the left and right columns. Optimal least squares fits to the logarithmic and fractional linear functions of Table 4 are overlaid on the data points in the left and right columns respectively. Traces A and B are from an experiment where the cell was subject to 20 mM cobalt; trace A: $I_{ext} = 4$ nA, trace B: $I_{ext} = 5$ nA. For traces C and D cobalt was absent; trace C: $I_{ext} = 2.6$ nA, trace D: $I_{ext} = 2.8$ nA. The sum of the norm of the residuals divided by the number of data points for each pair of fits are as follows. (The first value is for the logarithmic fit and the second for the fractional linear fit.) A: 0.0666, 0.0642; B: 0.0322, 0.0368; C: 0.0647, 0.0630; D: 0.0650, 0.0658.

are shown in Figure 15. Two of these traces come from experiments done in the presence of 20 mM Cobalt, which blocks the calcium currents in the LP cell. It should be noted that in all of the traces shown in Figure 15 (and indeed, in virtually all of the terminating traces that we analyzed), the "step" feature described above is, although less pronounced than in the model, clearly visible. This suggests that the LP cell achieves termination of firing by passage through a subcritical Hopf bifurcation close to a homoclinic orbit of focal type and that this mechanism is independent of calcium. As described above, there are two contributing factors for spike frequency adapta-

tion as a system approaches such a bifurcation: the magnitude of the real part of the unstable eigenvalue and the distance of closest approach to the equilibrium. The first of these factors would dictate that the spike frequency should behave as a fractional linear function as termination is approached, while the second would indicate a logarithmic function. Fits for both of these types of functions are shown in Figure 15 and the corresponding error measures are indicated in the caption. As can be seen, both of these types of functions had approximately the same success in fitting the data. In contrast, fits of this data to the square root function predicted by the saddle-node

termination scenario (not shown) were approximately twice as bad.

5. Discussion

The timing of action potentials is critical for the functioning of central pattern generators in neural systems. In systems with a time scale slower than that associated with periodic spiking, the onset and termination of spiking can be associated with bifurcations that occur when the slow time scale has been "frozen." Mathematically, the neural system is viewed as a singularly perturbed system. Rinzel (1987), Wang and Rinzel (1995) and Bertram et al (1995) have given topological characterizations of bursting patterns in terms of singularly perturbed systems. This analysis allows many bursting patterns associated with different bifurcations to be distinguished, but there are some cases in which the underlying dynamical mechanisms can only be determined by quantitative analysis. We consider two such mechanisms here, the termination of spiking via homoclinic bifurcations and saddle-node bifurcations of equilibria that interrupt a cyclic oscillation. In each of these cases, the frequency of oscillation slows as one approaches the termination of spiking. We analyze the rate at which the frequency of oscillation slows in the two cases and illustrate our analysis on neuronal models. We then apply the asymptotic analysis to experimental data on the LP neuron, leading to a tentative conclusion that the dynamical mechanism associated with termination of spiking in this cell lies close to a subcritical Hopf bifurcation with a homoclinic orbit of focal type. Although the logarithmic relation predicted by the homoclinic termination scenario fit the data as well as the fractional linear fit, the steps in decrease of instantaneous spike frequency support the subcritical Hopf scenario. We have not investigated whether these apparent steps of instantaneous spike frequency might be due to stochastic effects. There is sufficient noise in the subthreshold regions of the data to mask growing oscillations that would provide further evidence for the Hopf scenario. The LP neuron data are not well fit by the square root function, suggesting that, at least with the experimental conditions we employed, adaptation and spike termination

does not occur by a saddle-node bifurcation. Note that slow adaptation was similar both in normal saline (Figures 15C and 15D) and in saline with 20 mM Co^{2+} to eliminate Ca^{2+} currents (Figures 15A and 15B). Most models of slow spike frequency adaptation depend at least in part on intracellular Ca^{2+} accumulation and activation of Ca^{2+}-dependent outward currents (see, for example, Hartline and Graubard, 1992). Our results show that the very slow component of spike frequency adaptation in the LP cell does not depend on Ca^{2+} currents.

We can make further predictions about neuronal behavior associated with homoclinic and saddle-node bifurcations in a frozen system. Homoclinic bifurcations are associated with bistability in a system. A typical behavior in systems with homoclinic bifurcation is that following the bifurcation, the system evolves to a stable state that is far from the oscillatory cycle. This new stable state is one that existed for some range of parameters prior to the bifurcation, so one expects that there is a parameter range in which the system shows bistability. In contrast, saddle-node bifurcations often occur in systems where there is a single attracting stable state for each value of the parameters. It may be possible to find evidence for bistability or its absence in slowly varying systems by subjecting the systems to brief disturbances (e.g., current pulses) that alter the state of the system. If there is bistability, appropriate disturbances will move the system from the basin of attraction of one stable state to that of the other. The LP cell shows marked bistability, as manifest in very slow bursting to plateau oscillations, in the presence of Co^{2+} over a limited range of external current injection, as well as in the presence of dopamine (Peck and Harris-Warrick, unpublished). This further supports the location of the LP cell near a homoclinic bifurcation.

References

1. V. I. Arnold, V. S. Afrajmovich, Yu. S. Ilyashenko, L. P. Shilnikov (1994), Dynamical Systems V, Springer-Verlag.
2. L. A. Belyakov (1974), A case of the generation of periodic motion with homoclinic curves, Math. Notes of the Acad. Sci. USSR, 15, 336-341.
3. R. Bertram, M. J. Butte, T. Kiemel and A. Sherman (1995), Topological and phenomenological classifica-

tion of bursting oscillations, Bull. Math. Biology, 57, 413-449.

4. M. Bosch and C. Simo (1993), Attractors in a Silnikov-Hopf scenario and a related one dimensional map, Phys. D, 62, 217-229.

5. F. Buchholtz, J. Golowasch, I. Epstein and E. Marder (1992). Mathematical model of an identified stomatogastric ganglion neuron, J. Neurophysiol. 67:332-339.

6. B. Deng and K. Sakamoto (1995), Silnikov-Hopf bifurcations, J. Diff. Eq. 119, 1-23.

7. B. Ermentrout and N. Kopell (1986), Parabolic bursting in an excitable system coupled with a slow oscillation, Siam J. App. Math, 46, 233-253.

8. N. Fenichel (1971), Persistence and smoothness of invariant manifolds for flows, Indiana Univ. Math. J. 21, 193-226.

9. R. E. Flamm and R. M. Harris-Warrick (1986), Aminergic modulation in the lobster stomatogastric ganglion, J. Neurophysiol., 55, 847-881.

10. P. Glendinning and C. Sparrow (1984), Local and global behavior near homoclinic orbits, J. Statist. Phys., 34, 645-696.

11. J. P. Golowasch (1991). Characterization of a stomatogastric ganglion neuron. A biophysical and mathematical interpretation. Thesis, Brandeis University.

12. J. Guckenheimer and P. Holmes (1983), Nonlinear Oscillations, Dynamical Systems, and Bifurcation of Vector Fields, Springer Verlag.

13. R. Harris-Warrick, L. Coniglio, R. Levini, S. Gueron and J. Guckenheimer (1995), Dopamine modulation of two subthreshold currents produces phase shifts in activity of an identified neuron, J. Neurophysiol. 74, 1404-1420.

14. D. Hartline and K. Graubard (1992), Cellular and synaptic properties in in the crustacean stomatogastric nervous system, in Dynamic Biological Networks, R. Harris-Warrick, E. Marder, A. Selverston and M. Moulins, eds., MIT Press, 31-86.

15. B. Hille (1992), Ionic Channels of Excitable Membranes, Sinauer.

16. P. Hirschberg and E. Knobloch (1993), Silnikov-Hopf bifurcation, Phys. D, 62, 202-216.

17. Yu. S. Ilyashenko and S. Yu. Yakovenko (1991), Finitely-smooth normal forms of local families of diffeomorphisms and vector fields, Russian Math Surveys, 46, 1-43.

18. E. F. Mishchenko and N. Kh. Rozov (1980), Differential equations with a small parameter multiplying the highest derivative and relaxation oscillations, Plenum Press.

19. A. I. Nejshtadt Asymptotic investigation of the loss of stability as a pair of eigenvalues slowly cross the imaginary axis, Usp. mat. Nauk 40, 190-191, 1985.

20. S. Newhouse (1979), The abundance of wild hyperbolic sets and non-smooth stable sets for diffeomorphisms, Publ. Math. I.H.E.S., 50, 101-151.

21. J. Rinzel (1987), A formal classification of bursting mechanisms in excitable systems, Proc. Intern. Congr. of Mathematicians (A.M. Gleason, ed.), Amer. Math. Soc., 1578-1594.

22. J. Rinzel and B. Ermentrout (1989), Analysis of neural excitability and oscillations, in Methods of Neural Modeling : From Synapses to Networks, C. Koch and I. Segev, eds., MIT Press, 135-169.

23. J. Rinzel and W. Troy (1982), Bursting phenomena in a simplified Oregonator flow model, J. Chem. Phys. 76, 1775-1789.

24. A. I. Selverston, D. F. Russell, J. P. Miller and D. G. King, The stomatogastric nervous system: Structure and function of a small neural network, Prog. Neurobiol. 7, 215-290.

25. L. Shilnikov and D. Turaev (1995), On blue sky catastrophes, Doklady Academii Nauk, v.342, 596-599.

26. X.-J. Wang and J. Rinzel (1995), Oscillatory and bursting properties of neurons, The Handbook of Brain Theory and Neural Networks, M. Arbib, ed. MIT Press, 686-691.